International Journal of Science and Research (IJSR)
ISSN (Online): 2319-7064
Index Copernicus Value (2013): 6.14 | Impact Factor (2013): 4.438

Numerical Study on Aerodynamic Wave Drag Reduction by Counterflow Supersonic Jet in Hypersonic Flow

Shyam Kanwar[1], Mahendra Singh[2], Shatrughan Jaiswal[3] and Gouri Shankar Kanday[4]

[1, 3, 4] Institute of Technology, Guru Ghasidas University, Department of Mechanical, Koni, Bilaspur 495006, India
[1]*shmkanwar21@gmail.com*
[3]*spjshatrujaiswal@gmail.com*
[4]*gourishankarkhanday@gmail.com*
[2]Christian College of Engineering and Technology, Department of Mechanical, Bhilai 490026, India
[2]*msk.gsk21@gmail.com*

Abstract: ***A numerical study on the reduction of aerodynamic wave drag by counterflow jet in hypersonic flow has been conducted. In the present study, dimensional axisymmetric Euler equations are used as governing equation. Analysis has been carried out for an axisymmetric 60^0 apex-angle blunt module with and without injection cooling since Mach number of 8.0. The spatial discretization is carried out by unstructured cell-centered Finite Volume Method. Here the convective fluxes are evaluated using Van Leer Flux Splitting Scheme. Species transport equations are also added in the Euler equation for treatment of non-reacting mixing of the coolant gas. The numerical code has been successfully validated using standard experimental data for counter flow injection. The numerical result shows about 16%–42% reduction in drag coefficient for different jet pressures. It becomes clear that a performance of the reduction of aerodynamic wave drag by opposing jet is greatly affected by jet condition.***

Keywords: Hypersonic flow, supersonic jet, Aerodynamics wave drag, Finite Volume Method, Van Leer Flux Splitting schemes.

1. Introduction

The aerodynamic phenomenon associated with very high speed flight, such as those which is encountered during atmospheric reentry of space flights, is classified as hypersonic aerodynamics. Hypersonic aerodynamics are different from supersonic or subsonic aerodynamics. The Hypersonic region of the flight is generally accepted when the Mach number exceeds 5 where the aerodynamic wave drag and heating becomes important in aircraft design.

One of the major examples of the effect of aerodynamic heating is the failure of the Columbia Space Shuttle during re-entry in 2003 [1]. The physical cause of the loss of Columbia and its crew was a breach in the Thermal Protection System on the leading edge of the left wing.

Currently, developments of Reusable Launch Vehicle (RLV) for a low cost space transportation system are in progress [2]. In the development of RLV, one of the most important problems is the severe aerodynamic heating and wave drag at the nose and leading edges of the vehicle.

In recent years, there has been strong interest in using forward facing supersonic jet emanating from the stagnation point of a blunt body to reduce wave drag and heat flux flying as hypersonic Mach number. Zheng et al. [3], Nair et al.[4] And Yisheng [5] conducted some numerical analysis and experiments to investigate the wave drag and thermal load reduction by counter-flowing jets.

Present research work also revealed drag reduction by counterflowing supersonic jet for 60° apex angle blunt cone is investigated numerically using CFD. A schematic representation of the flow field flow field features around the blunt cone with a counter flowing jet is shown in Figure.1.

The counter flow jet separates from the sharp edged orifice. The jet expands till a mach disc is formed and thereafter it turns in the direction of the mainstream.

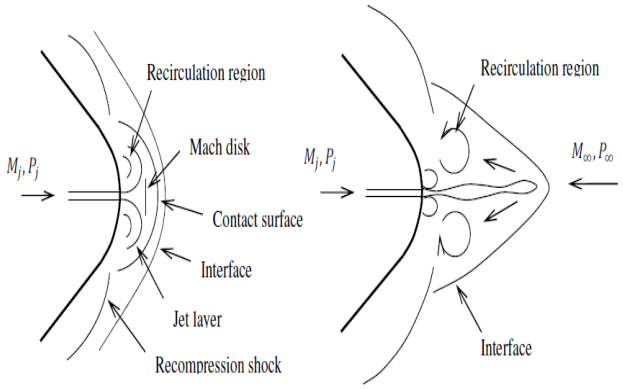

Figure 1: Schematic representation of flow field induced by injection cooling forward of blunt body

Due to the low pressure created by expansion of the jet, a recirculation region is formed in the shear layer. The jet layer mixes with a shear layer of mainstream only after this recirculation region thereby forming a dividing stream surface. The jet layer turns along the body surface flows along downstream. The pressure rise associated with the reattachment of the shear layer causes a recompression shock in the jet layer and the flow from the mainstream outside the interface. Hence the shear surface turns downstream from the intersection of the recompression shock with the main bow shock.

2. Governing Equations

For high speed flows, viscous effect is confined to the vicinity of the surface, where the large velocity gradient exists. This region is known as the boundary layer. Outside

of the boundary layer, the velocity gradients are negligible resulting in zero shear stress. This region is called the inviscid region. In the present study, the investigation of solution procedures for the inviscid flow region. The governing equation is known as the Euler equation [6]. In two-dimensional Cartesian coordinates, these can be written as

$$\frac{\partial \vec{U_i}}{\partial t}+\frac{\partial \vec{F_i}}{\partial x}+\frac{\partial \vec{G_i}}{\partial y}=0 \quad (1)$$

$$\vec{U}_i=\begin{bmatrix}\rho\\ \rho u\\ \rho v\\ \rho E\\ \rho m_i\end{bmatrix} \quad \vec{F_i}=\begin{bmatrix}\rho u\\ \rho u^2+p\\ \rho uv\\ \rho uH\\ \rho um_i\end{bmatrix} \quad \vec{G_i}=\begin{bmatrix}\rho u\\ \rho uv\\ \rho v^2+p\\ \rho uH\\ \rho vm_i\end{bmatrix}$$

The Euler equations governing the 2D flow in the absence of body forces with species transport equation in the conservative and differential form are,

$$\frac{\partial(\rho)}{\partial t}+\frac{\partial(\rho u)}{\partial x}+\frac{\partial(\rho v)}{\partial y}=0 \quad (2)$$

$$\frac{\partial(\rho u)}{\partial t}+\frac{\partial(\rho u^2+p)}{\partial x}+\frac{\partial(\rho v)}{\partial y}=0$$

(3)

$$\frac{\partial(\rho E)}{\partial t}+\frac{\partial(\rho uH)}{\partial x}+\frac{\partial(\rho vH)}{\partial y}=0 \quad (4)$$

$$\frac{\partial(\rho m_i)}{\partial t}+\frac{\partial(\rho um_i)}{\partial x}+\frac{\partial(\rho vm_i)}{\partial y}=0 \quad (5)$$

In the above versions of formulations, the total specific energy, $E=e+0.5(u^2+v^2)$ the total specific enthalpy $H=h+0.5(u^2+v^2)$, is the mass fraction of the species given by $m_i=\rho_i/\rho$. For the mixtures of gases, the perfect gas relations can be used together with the effective thermodynamic properties or the mixtures of the gas, can be used the perfect gas relations together with the effective thermodynamic properties.

$$R=\sum M_i R_i \quad , \quad \gamma=\sum M_i \gamma_i$$

This thesis considers a solution to unsteady state Euler equations and no surface forces are considered in these equations. Euler equation basically expresses the conservation of mass, momentum and energy.

3. Numerical Method

3.1 Finite volume method formulation

The basic idea of a FVM is to satisfy the integral form of the conservation laws to some degree of approximation for each of many adjacent control volumes which cover the domain of interest.

$$\frac{d}{dt}\int_{V(t)}\overline{U}dV+\iint_{S(t)}\vec{n}.\vec{F}ds=0 \quad (5)$$

The average value of U in a cell with volume V is

$$\overline{U}=\frac{1}{V}\iint UdV \quad (6)$$

Eq. 3.1 can be written as

$$V\frac{d}{dt}\overline{U}+\iint_{S(t)}\vec{n}.\vec{F}ds=0 \quad (7)$$

$$\frac{d\overline{U}}{dt}+\frac{1}{V}\iint_{S(t)}\vec{n}.\vec{F}ds=0 \quad (8)$$

$\overline{U}$ is the average value of U over the entire control volume, $\vec{F}$ is the flux vector and $\vec{n}$ is the unit normal to the surface. And $\vec{F}=F_I\vec{i}+G_I\vec{j}$, is the total inviscid flux, upon integrating the inviscid flux over the faces of k^{th} control volume the above equation becomes

$$\frac{\partial U_k}{\partial t}+\frac{1}{V_k}\left[\sum_{i=1}^{nf}\vec{F}.\vec{n}ds\right]_k=0 \quad (9)$$

Here, $\vec{n}=\frac{\Delta y_i}{\Delta s_i}\vec{i}-\frac{\Delta x_i}{\Delta s_i}\vec{j}$ and $\Delta s_i=\sqrt{(\Delta x)_i^{\,2}+(\Delta y)_i^{\,2}}$

For the 2-D axi-symmetric problems the finite volume formulation is given by

$$\frac{d\overline{U}}{dt}+\frac{1}{V}\iint_{S(t)}\vec{n}.\vec{F}ds=S \text{ , here } S=-\frac{1}{r}\begin{bmatrix}\rho v\\ \rho uv\\ \rho v^2\\ (e+p)v\end{bmatrix}$$

3.2 Upwind discretization

Upwind schemes use an adaptive or solution-sensitive finite difference stencil to numerically simulate the direction of propagation of information in a flow field. A general form of writing any upwind-type schemes are

$$u_i^{n+1}=u_i^n-\frac{a\Delta t}{\Delta x}[(u_i^n-u_{i-1}^n)+(u_{i+1}^n-u^n{}_i)] \quad (10)$$

The upwind scheme is stable if the following Courant Friedrich–Lewy condition (CFL) condition is satisfied. Here CFL condition is $|a\Delta t/\Delta x|\le 1$. The scheme is first order accurate explicit scheme with only one unknown u_i^{n+1}.

3.3 Van Leer flux splitting scheme

The Van Leer scheme tells general fluid flow contains wave speeds that are both positive and negative (so that eigenvalue information can pass both upstream and downstream), the basic idea behind all of these techniques is that the flux can be split into two components F^+ and F^- so that each may be properly discretized using relatively upwind stencils to maintain stability and accuracy [7].

If $M_\perp \geq 1$, then $F^+_\perp = F_\perp, F_\perp^- = 0$

If $M_\perp \leq -1$, then $F^-_\perp = F_\perp,\ F_\perp^+ = 0$

If $-1 < M_\perp < 1$ then numerical normal flux $F_\perp = F_\perp^+(U_L) + F_\perp^-(U_R)$

$$F_\perp = \begin{bmatrix} \rho u_\perp \\ \rho u_\perp u + p n_x \\ \rho u_\perp v + p n_y \\ \rho u_\perp H \\ \rho u_\perp m_i \end{bmatrix}$$

$$\vec{F}_\perp^{\pm} = \pm\frac{\rho c(1 \pm M_\perp)^2}{4} \begin{bmatrix} 1 \\ u \pm (-M_\perp \pm 2)\frac{c}{\gamma^\pm} n_x \\ v \pm (M_\perp \pm 2)\frac{c}{\gamma^\pm} n_y \\ \frac{q^2 - u_\perp^{\ 2}}{2} + \frac{c^2}{2(\gamma^\pm + 1)}\left[(\gamma^\pm - 1)M_\perp \pm 2\right]^2 \\ m_i \end{bmatrix}$$

3.4 Boundary conditions

Boundary conditions are specifications of properties or conditions on the surfaces of fluid domains and sub-domains, and are required to fully define the flow simulation. Boundary condition decides the solution of the governing equation.

For two dimensional inviscid flow problem the commonly encountered boundary conditions are, 2D solid boundary fluxes, Inviscid or slip wall boundary condition, Pressure extrapolation boundary condition, Mirror image boundary condition, Far field boundary condition.

3.5 Grid and flow conditions

A typical grid used for the computations of flow fields around 60^o Apex-angle blunt body model [8] with 2 mm jet diameter in the nose region, which are shown in Figure 2.

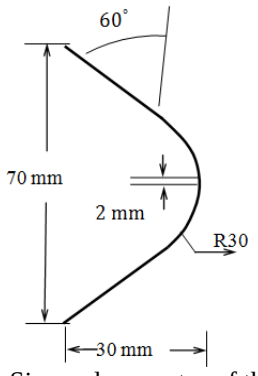

Figure 2: Size and geometry of the blunt

The flow is assumed to be axisymmetric for blunt cone, then only half of the geometry need for simulation, instead of 3D models. Figure 3 shows the grid system used in the present study. The number of grid points is 205 in the x- direction (along the body) and 150 in the y- direction (perpendicular to the body). 6 points in the y- direction are distributed to express the exit of the coolant gas at the nose of the body. Flow conditions are shown in Table 1 and Table 2.

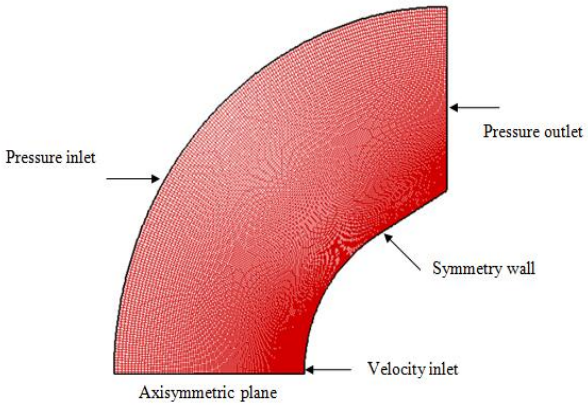

Figure 3: Boundary conditions and computational domain (205×150)

Table 1: Flow condition of free stream

Fluid	*Static pressure (Pa)*	*Static temperature (K)*	*Mach number*	*Velocity (m/s)*
Air	284.0	316.0	8.0	2850.62

Table 2: Flow condition of supersonic jet (coolant gas)

Gas	*Total pressure (bar)*	*Total Temperature (K)*	*Mach number*
Air/Helium	2.0	300.0	1.0
	4.0	300.0	1.0
	6.0	300.0	1.0
	8.0	300.0	1.0

4. Solver Validation

4.1 Supersonic flow over a cylinder

The inviscid flow past a cylinder of radius 30 mm has been investigated for Mach number 8.The fluid domain geometry with mesh is shown in Figure 4(a). The important flow feature consists of bow shock wave detached from the body which is normal shock at the nose becoming weak downstream. Behind the normal portion of the shock wave flow is subsonic which during expansion becomes supersonic over the cylinder. Thus the flow in the shock layer is mixed subsonic supersonic flow as seen in the typical Mach counter Figure 4(b).

In all test cases mentioned above, the solver code has to give an approximate match with the various theories in hypersonic flow. For flow past a cylinder validates the shock wave shape using Billig correlation [9].

The validation studies of the flow solver are carried for Mach number (M=8) to predict the variation of shock stand-off distance with Mach number. The shock detachment distance obtained from the solver has been compared with Billig correlation for shock detachment distance, which is given by for cylinder,

$$\frac{\delta}{R} = 0.386 \exp\left(\frac{4.67}{M_\infty^2}\right), \quad \frac{R_c}{R} = 1.386 \exp\left(\frac{1.8}{(M_\infty - 1)^{0.75}}\right)$$

The studies are further extended to predict the shock wave shape from the solver is validated with the empirical correlation given by

$$x = R + \delta - R_c \cot^2 \beta \left[\left(1 + \frac{y^2 \tan^2 \beta}{R_c}\right)^{1/2} - 1\right] \quad (13)$$

Table 3: Comparison of various parameters across shock (cylinder)

Parameter	*Normal shock theory*	*Solver Result*
P_2/P_1	74.50	74.72
T_2/T_1	13.38	13.41
ρ_2/ρ_1	5.56	5.53
M_2	0.39	0.37

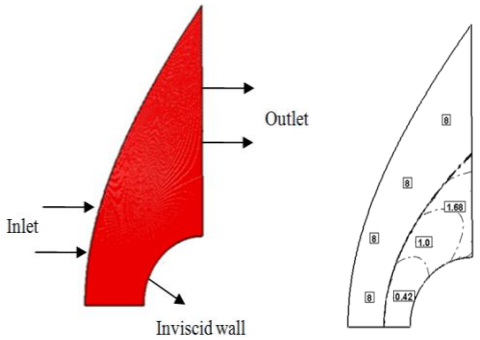

"(a)" "(b)"

Figure 4: Computational domain for flow past cylinder

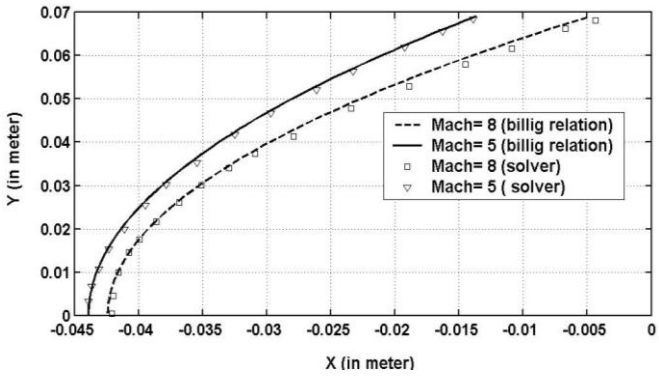

Figure 5: Comparison of shock wave shape using Billig correlation for cylinder

5. Result and Discussion

5.1 Counterflow supersonic jet in hypersonic flow

Following procedures as mentioned in previous sections, numerical result are obtained for drag force computations with supersonic jet injection are carried out for four different injection pressure ratios $(P_{0j}/P_{0\infty})$, that is namely 7.45, 14.91, 22.36 and 29.82 which correspond to 2, 4, 6 and 8 bar stagnation pressure of the jet. These numerical results lead to various forms of outputs. Effects of total pressure ratio, graphical representation and contour representations are the significant results obtained from the current analysis.

5.2 Formulation for wave drag coefficient

To determining the wave drag coefficient at the body it is clarify the reduction of drag force due to injection cooling. Drag, the fluid dynamics refers to forces which act on a solid object in the direction of the relative fluid flow velocity. The net drag is approximated by a non dimensional parameter called wave drag coefficient which is defined by

$$C_d = \frac{2F_d}{\rho_\infty V_\infty^2 A} = \frac{1}{\rho_\infty V_\infty^2 A} \int_s (P - P_\infty).\vec{n}.dA \quad (14)$$

Table 4: Drag coefficient for various injection pressure of jet (with air as coolant gas)

Injection pressure (bar)	*Coefficient of drag (C_d)*	*Reduction in C_d (%)*
0	0.8717	-----
2.0	0.7567	13.2%
4.0	0.6506	25.4%
6.0	0.5875	32.6%
8.0	0.5322	38.9%

Table 5: Drag coefficient for various injection pressure of jet (with helium as coolant gas)

Injection pressure (bar)	*Coefficient of drag (C_d)*	*Reduction in C_d (%)*
0	0.8717	-----
2.0	0.7256	16.7%
4.0	0.6699	23.1%
6.0	0.5689	34.7%
8.0	0.501	42.5%

5.3 Contour representations

Figure 6 and Figure 7 show the contour of Mach number for $60°$ apex angle blunt configuration in the absence of jet and in the presence of jet. From the Figure 6 clear that strong bow shock wave originates at the nose region that reduces the speed of the body. This causes a higher amount of drag at the nose region. Figure 7 displays the contours of Mach number to survey the actually existing amount of drag over the body in the presence of jet. Mach contour for total pressure ratios.

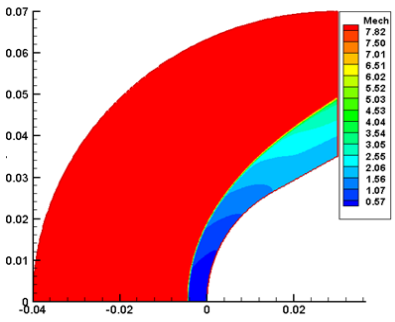

Figure 6: Mach number contour in the absence of jet

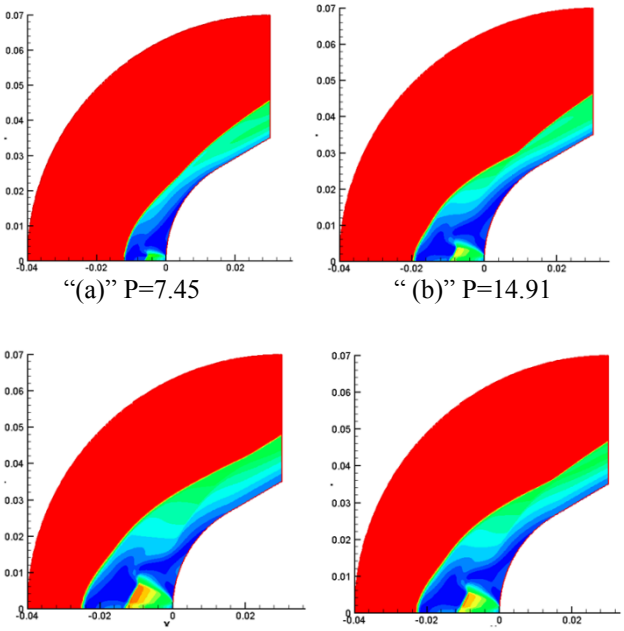

"(a)" P=7.45 " (b)" P=14.91

"(c)" P=22.36 "(d)" P=29.82

Figure 7: Mach number contour at various P

A larger recirculation region has formed at the blunt region. This larger recirculation region expels the bow shock far away from the nose region and enlarges the shock stand-off distance. The jet coming out from the blunt nose with the high velocity pushes the bow shock away from the blunt region of the body. This shows the way to reduction in drag.

5.4 Effects of total pressure ratio

Figure 8 and Figure 9 show temperature contours for air and helium injection respectively. As the total pressure ratio increases, a mass flow ratio of jet increases and a shape of bow shock wave changes. As a result, cool supersonic jet flows which pass through bow shock wave increase. Due to jet, the main stream flows outside of cool supersonic jet flow, and then it passes through recompression shock wave. Observing temperature contours, temperature around a reattachment point increases. Temperature around a reattachment point decreases as the total pressure ratio increases. This is caused by cool jet flow near the wall. With the increase of total pressure ratio, the area of recirculation region increases and the position of reattachment point moves away from the stagnation point. This is the reason why the temperature of recirculation region decreases.

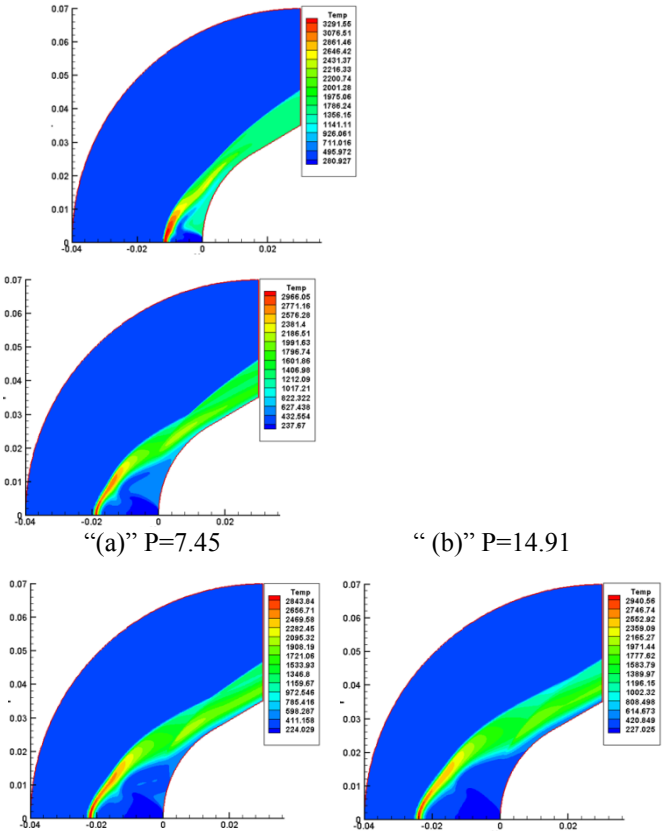

"(a)" P=7.45 " (b)" P=14.91

"(c)" P=22.36 "(d)" P=29.82

Figure 8: Temperature contour at various P with air injection

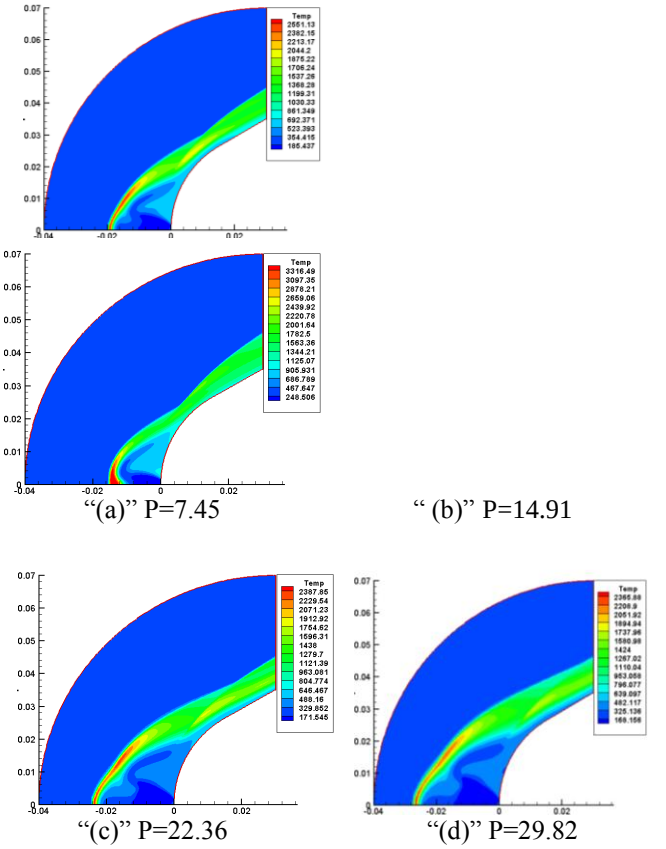

"(a)" P=7.45 " (b)" P=14.91

"(c)" P=22.36 "(d)" P=29.82

Figure 9: Temperature contour at various P with helium injection

5.5 Graphical representations

The graphical representation of pressure drag and static pressure distribution which illustrate the comparative study between the case in the absence of jet and in the presence of jet for the blunt body are given here. The optimum condition for jet which is given in the Table 2 have been executed in the presence of the jet case, for 60° apex angle blunt body which is consider in the present work. The comparison of static pressure distribution in the absence of jet and in the presence of jet, with different jet conditions is presented through Figure 10, From the figure, very high amount of static pressure distribution is clearly seen at the nose region in without injection case. And in the injection case, evaluation of the static pressure distribution shows the nose static pressure distribution is minimum at the tip then slightly increases due to recompression shock wave.

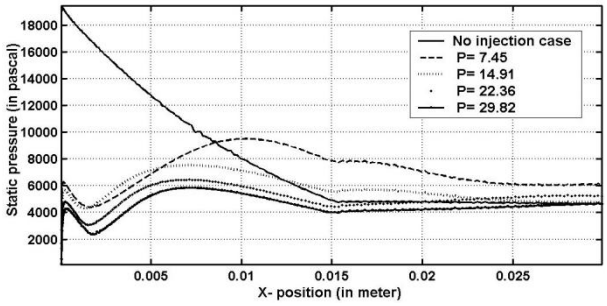

Figure 10: Comparison plot of static pressure distribution between with and without injection case

Hence, the reduction of static pressure distribution over the wall is clearly observed on the blunt cone configuration. Figure 11 and Figure 12 show drag reduction on the body of each total pressure ratio. Mach number of jet is unity (M_{∞}=1) at jet exit. As the total pressure ratio increases, the drag coefficient decreases.

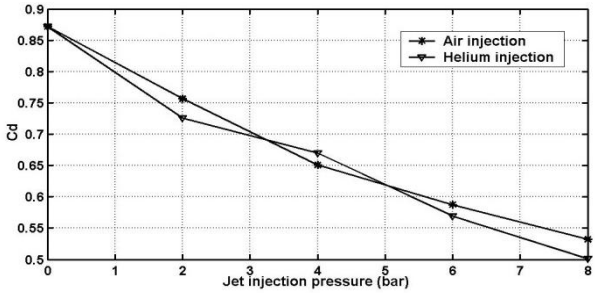

Figure 11: Variation of drag coefficient with the injector pressur

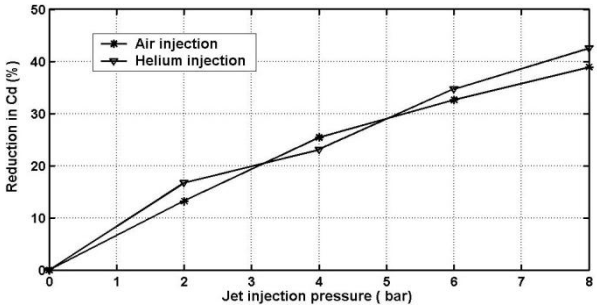

Figure 12: Percentage of drag reduction as a function of injector pressure

6. Conclusion

In the present study, drag reduction in hypersonic flow with counterflow jet is investigated with CFD. The detailed flow field with counterflow jet in hypersonic flow is calculated by solving dimensional axisymmetric Euler equation. The numerical results are validated with experiments. The remarkable drag reduction is observed when the opposing jet flows. The numerical result shows about 16%–42% reduction in drag coefficient for different jet pressures. It becomes clear that a performance of the reduction of aerodynamic wave drag by opposing jet is greatly affected by jet condition.

References

[1] Columbia (2006). Report of Columbia Accident Investigation Board. *Accident Investigation Board* 1, 78-82.

[2] Suresh, M. R. (2008). Materials Development for Future Reusable Launch Vehicles. *International Conference on Aerospace Science and Technology Bangalore India*.

[3] Zheng, Y., N. A. Ahmed, and W. Zheng (2012). Heat dissipation using minimum counterflow jet ejection during spacecraft re-entry. *Procedia Engineering* 49, 271-279.

[4] Nair, P., T. Jayachandranl, M. Deepu, B.P. Puranik and U.V. Bhandarkar (2010). Numerical Simulation of Interaction of Sonic Jet with High Speed Flow over a Blunt Body using Solution Mapped Higher Order Accurate AUSM+-UP Based Flow Solver. *Journal of Applied Fluid Mechanics* 3, 15-23.

[5] Yisheng, R. (2013). Drag reduction research in supersonic flow with opposing jet. *Acta Astronautica* 91, 1-7

[6] Anderson, J. D. (1989). Hypersonic and High Temperature Gas Dynamics. *McGraw-Hill Inc*.

[7] Liou, M. S. and C. J. Steffen (1999). A New Flux Splitting Scheme. *Journal of Computational Physics* 107, 23-39.

[8] Sahoo, N., V. Kulkarni, S. Saravanan, G. Jagadeesh, and K. P. Reddy (2005). Film cooling effectiveness on a large angle blunt cone flying at hypersonic speed. *Physics of Fluids* 17, 036101- 036106

[9] Billig, F. S. (1968). Shock-wave shapes around spherical and cylindrical nosed Bodies. *Journal of Spacecraft Rockets* 5, 1247-1248.

Author Profile

Shyam Singh kanwar received the B.E. degrees in Mechanical Engineering from Government Engineering College Raipur in 2011 and M.Tech degree in Fluids & Thermal Engineering form Indian Institute of Technology Guwahati in 2013.